Research Article | Vol. 25, No. 4 | 20 Feb 2017 | OPTICS EXPRESS 3077

Optics EXPRESS

Coherent emission from integrated Talbot-cavity quantum cascade lasers

BO MENG,[1,2] BO QIANG,[1,3,4] ETIENNE RODRIGUEZ,[1] XIAO NAN HU,[1] GUOZHEN LIANG,[1,2] AND QI JIE WANG,[1,3,*]

[1]*Centre for OptoElectronics and Biophotonics, School of Electrical and Electronic Engineering & The Photonics Institute, Nanyang Technological University, Singapore, 639798, Singapore*
[2]*CINTRA CNRS/NTU/THALES, UMI 3288, Research Techno Plaza, 50 Nanyang Drive, Border X Block, Level 6, 637553, Singapore*
[3]*Centre for Disruptive Photonic Technologies, School of Physical and Mathematical Sciences, Nanyang Technological University, Singapore, 637371, Singapore*
[4]*Optoelectronics Research Centre, University of Southampton, Southampton SO17 1BJ, UK*
[*]*qjwang@ntu.edu.sg*

Abstract: We report experimental realization of phase-locked quantum cascade laser (QCL) array using a monolithically integrated Talbot cavity. An array with six laser elements at a wavelength of ~4.8 μm shows a maximum peak power of ~4 W which is more than 5 times higher than that of a single ridge laser element and a slope efficiency of 1 W/A at room temperature. Operation of in-phase coherent supermode has been achieved over the whole dynamic range of the Talbot-cavity QCL. The structure was analysed using a straightforward theoretical model, showing quantitatively good agreement with the experimental results. The reduced thermal resistance makes the structure an attractive approach to achieve high beam quality continuous wave QCLs.

OCIS codes: (140.5965) Semiconductor lasers, quantum cascade; (140.3298) Laser beam combining; (140.3290) Laser arrays.

References and links

1. R. Martini, C. Bethea, F. Capasso, C. Gmachl, R. Paiella, E. A. Whittaker, H. Y. Hwang, D. L. Sivco, J. N. Baillargeon, and A. Y. Cho, "Free-space optical transmission of multimedia satellite data streams using mid-Infrared quantum cascade lasers," Electron. Lett. **38**(4), 181–183 (2002).
2. A. P. M. Michel, P. Q. Liu, J. K. Yeung, P. Corrigan, M. L. Baeck, Z. Wang, T. Day, F. Moshary, C. F. Gmachl, and J. A. Smith, "Quantum cascade laser open-path system for remote sensing of trace gases in Beijing, China," Opt. Eng. **49**(11), 111125 (2010).
3. B. Guo, Y. Wang, C. Peng, H. Zhang, G. Luo, H. Le, C. Gmachl, D. Sivco, M. Peabody, and A. Cho, "Laser-based mid-infrared reflectance imaging of biological tissues," Opt. Express **12**(1), 208–219 (2004).
4. Y. Bai, S. R. Darvish, S. Slivken, P. Sung, J. Nguyen, A. Evans, W. Zhang, and M. Razeghi, "Electrically pumped photonic crystal distributed feedback quantum cascade lasers," Appl. Phys. Lett. **91**(14), 141123 (2007).
5. B. Gökden, T. S. Mansuripur, R. Blanchard, C. Wang, A. Goyal, A. Sanchez-Rubio, G. Turner, and F. Capasso, "High-brightness tapered quantum cascade lasers," Appl. Phys. Lett. **102**(5), 053503 (2013).
6. S. Menzel, L. Diehl, C. Pflügl, A. Goyal, C. Wang, A. Sanchez, G. Turner, and F. Capasso, "Quantum cascade laser master-oscillator power-amplifier with 1.5 W output power at 300 K," Opt. Express **19**(17), 16229–16235 (2011).
7. S. Ahn, C. Schwarzer, T. Zederbauer, D. C. MacFarland, H. Detz, A. M. Andrews, W. Schrenk, and G. Strasser, "High-power, low-lateral divergence broad area quantum cascade lasers with a tilted front facet," Appl. Phys. Lett. **104**(5), 051101 (2014).
8. E. Kapon, J. Katz, and A. Yariv, "Supermode analysis of phase-locked arrays of semiconductor lasers," Opt. Lett. **9**(4), 125–127 (1984).
9. S. S. Wang and H. G. Winful, "Dynamics of phase-locked semiconductor laser arrays," Appl. Phys. Lett. **52**(21), 1774–1776 (1988).
10. D. Botez, "Monolithic phase-locked semiconductor laser arrays," in *Diode Laser Arrays*, D. Botez and D. R. Scifres, eds. (Cambridge University, 1994), pp. 1–67.
11. J. D. Kirch, C.-C. Chang, C. Boyle, L. J. Mawst, D. Lindberg III, T. Earles, and D. Botez, "5.5 W near-diffraction limited power from resonant leaky-wave coupled phase-locked arrays of quantum cascade lasers," Appl. Phys. Lett. **106**(6), 061113 (2015).

#281380 https://doi.org/10.1364/OE.25.003077
Journal © 2017 Received 22 Nov 2016; revised 18 Jan 2017; accepted 27 Jan 2017; published 6 Feb 2017

Optics EXPRESS

12. G. M. de Naurois, M. Carras, B. Simozrag, O. Patard, F. Alexandre, and X. Marcadet, "Coherent quantum cascade laser micro-stripe arrays," AIP Adv. **1**(3), 032165 (2011).
13. L. K. Hoffmann, M. Klinkmüller, E. Mujagić, M. P. Semtsiv, W. Schrenk, W. T. Masselink, and G. Strasser, "Tree array quantum cascade laser," Opt. Express **17**(2), 649–657 (2009).
14. A. Lyakh, R. Maulini, A. Tsekoun, R. Go, and C. K. N. Patel, "Continuous wave operation of buried heterostructure 4.6 μm quantum cascade laser Y-junctions and tree arrays," Opt. Express **22**(1), 1203–1208 (2014).
15. J. R. Leger, "Lateral mode control of an AlGaAs laser array in a Talbot cavity," Appl. Phys. Lett. **55**(4), 334–336 (1989).
16. A. Evans, S. R. Darvish, S. Slivken, J. Nguyen, Y. Bai, and M. Razeghi, "Buried heterostructure quantum cascade lasers with high continuous-wave wall plug efficiency," Appl. Phys. Lett. **91**(7), 071101 (2007).
17. D. Botez, "Array-mode far-field patterns for phase-locked diode laser arrays: coupled mode theory versus simple diffraction theory," IEEE J. Quantum Electron. **21**(11), 1752–1755 (1985).
18. D. Mehuys, K. Mitsunaga, L. Eng, W. K. Marshall, and A. Yariv, "Supermode control in diffraction coupled semiconductor laser arrays," Appl. Phys. Lett. **53**(13), 1165–1167 (1988).
19. D. Mehuys, W. Streifer, R. G. Waarts, and D. F. Welch, "Modal analysis of linear Talbot-cavity semiconductor lasers," Opt. Lett. **16**(11), 823–825 (1991).
20. J. Z. Wilcox, M. Jansen, J. Yang, G. Peterson, A. Silver, W. Simmons, S. S. Ou, and M. Sergant, "Supermode discrimination in diffraction-coupled laser arrays with separate contacts," Appl. Phys. Lett. **51**(9), 631–633 (1987).
21. C. J. Corcoran and F. Durville, "Talbot cavity redesigned for increased supermode discrimination with reduced loss," Opt. Lett. **40**(13), 2957–2960 (2015).
22. D. Paboeuf, G. Lucas-Leclin, P. Georges, N. Michel, M. Krakowski, J. Lim, S. Sujecki, and E. Larkins, "Narrow-line coherently combined tapered laser diodes in a Talbot external cavity with a volume Bragg grating," Appl. Phys. Lett. **93**(21), 211102 (2008).
23. L. Wang, J. Zhang, Z. Jia, Y. Zhao, C. Liu, Y. Liu, S. Zhai, Z. Ning, X. Xu, and F. Liu "Phase-locked array of quantum cascade lasers with an integrated Talbot cavity," https://arxiv.org/abs/1609.087 90.

1. Introduction

With considerable improvement in the performance, quantum cascade lasers (QCLs) have become important and reliable sources in the mid-infrared (MIR) spectral region for applications such as free-space communications [1], remote environmental sensing [2], and biological imaging [3]. For those applications, achieving both high coherent output power and diffraction limited beam quality are highly desired. Along this line, a number of different structures based on broad area QCLs have been proposed and studied, such as photonic crystal distributed feedback (PCDFB) lasers [4], master-oscillator power-amplifier (MOPA) [5,6] lasers, and lasers with tilted front facet [7]. Another promising technique to obtain high output powers while maintaining a good beam quality is to use the coherent phase-locked array structures which have been extensively studied in the near-infrared region [8–10]. Recently, these concepts have been extended to the MIR region using QCLs platforms. For instance, resonant leaky-wave coupled QCLs arrays have shown 5.5 W peak power in a near diffraction limit far-field pattern at wavelength of 8.36 μm [11]. However, to ensure high refractive index contrast, it requires regrowth of semiconductor material which significantly complicates the fabrication processes. In addition, while providing a better thermal management, evanescent-wave-coupled arrays tend to operate in the out-of-phase mode, leading to a double-lobe far-field pattern which is undesirable for practical applications [12]. Y-branch coupled arrays, on the other hand, often undergo strong modal competition between in-phase and out-of-phase modes although promising results have been recently reported under CW operation and stable phase-locked conditions [13, 14].

In this work, we report an alternative scheme based on diffraction coupling for implementation of phase-locked arrays using the Talbot-effect [15]. In the Talbot-effect, the amplitude distribution of a periodic source reimages itself at regular distances away from the source. The regular distance is called the Talbot length $Z_t = 2nd^2/\lambda_0$, where n is the refractive index of the material, d is the source period, and λ_0 is the wavelength of light in vacuum. In our structure, a Talbot cavity serving as the coherent in-phase coupling element is monolithically integrated with a periodic QCLs array. The proposed structure provides a

Optics EXPRESS

stable and near diffraction limit far-field pattern in the central lobe for in-phase supermode operation over the entire dynamic range.

2. Device fabrication

In the current experiments, the array section consists of six laser elements with a common width of 7.5 μm and an 11.5 μm center-to-center spacing. The schematic of the proposed structure is shown in Fig. 1(a). The devices were fabricated on an MBE-grown QCL structure with double-phonon-resonance active region design with a designed wavelength of 4.7 μm [16]. The whole structure was grown on an *n*-doped InP substrate, starting with the lower cladding layer [consisting of a 1.5 μm thick *n*-doped (8.5×10^{16} cm^{-3}) InP layer and a 1.5 μm thick *n*-doped (2.5×10^{16} cm^{-3}) InP layer], followed by the active region, the top cladding layer [consisting of a 1.5 μm thick *n*-doped (2.5×10^{16} cm^{-3}) InP layer and a 1.5 μm thick *n*-doped (8.5×10^{16} cm^{-3}) InP layer], and a thin 20 nm highly *n*-doped (1×10^{19} cm^{-3}) InGaAs cap layer. The active region consists of 40 periods of strained $Ga_{0.331}In_{0.669}As/Al_{0.638}In_{0.362}As$ pairs to enhance the band offset to ~800 meV for the designed wavelength. The devices were etched by inductively coupled plasma (ICP) reactor with an Ar/Cl_2 recipe using a SiO_2 hard mask. We have etched ~8 μm deep through the active region down to the substrate to avoid the evanescent coupling. The devices were then passivated with 550 nm SiO_2. After opening the top window, Ti/Au metal contact was evaporated using the electron beam evaporator. Extended Au contact was evaporated using a combination of sputtering and electroplating to provide better coverage of the devices sidewalls. The two sections of the Talbot-cavity and QCL array are electrically connected through the Au top contact. After substrate lapping, the deposition of Ti/Au bottom contact finished the whole process. The devices were cleaved in a

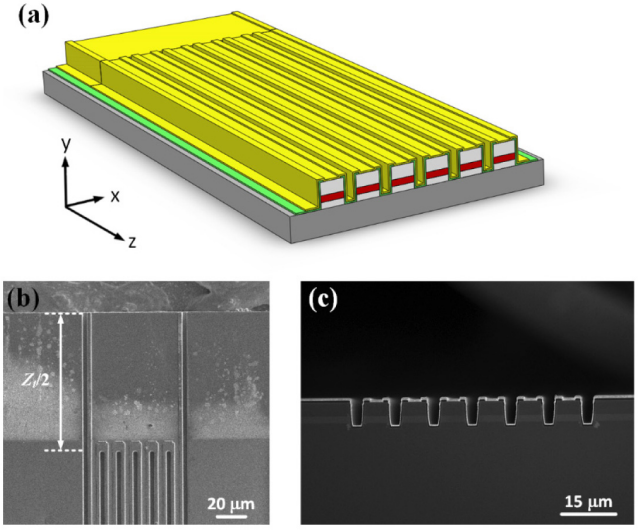

Fig. 1. (a) 3D schematic of the proposed Talbot-cavity quantum cascade lasers (QCLs), as well as representative SEM images of (b) the Talbot cavity with a half of the Talbot length Z_t /2 and (c) the output facet of the QCL array with six laser elements. Each element has a common width of 7.5 μm and an 11.5 μm center-to-center spacing.

way that Talbot cavity length varies from 30 μm to 100 μm. The as-cleaved devices were epilayer-up bonded on Cu heatsinks for testing. The representative scanning electron microscope (SEM) images of the fabricated Talbot cavity and the QCL array are shown in Figs. 1(b) and 1(c), respectively. For all the results presented here, the devices were tested in the pulsed mode operation, with a 100 ns pulse width and a 10 kHz repetition rate at a heatsink temperature of 300 K.

Optics EXPRESS

3. Results and analysis

Figure 2 shows the light-current (*L-I*) and light-voltage (*I-V*) characteristics of a representative Talbot-cavity QCL (with Talbot cavity of $Z_t/2$) as well as a Fabry-Perot (F-P) QCL (7.5 μm wide, 3.5 mm long) for comparison. For Talbot-cavity QCL, the output power was measured directly from the QCL array output facet using a thermopile detector. The slope efficiencies for the F-P and Talbot QCLs are 1.1 W/A and 1.0 W/A, respectively. The F-P QCL delivered a peak power of 0.75 W, whereas, for comparison, the Talbot-cavity QCL showed a peak power of 4 W, which scales almost linearly with the number of the devices of the array. Similar to the case of tapered QCLs, the threshold current density and slope efficiency of Talbot-cavity QCL cannot be described by the commonly used expression, which assumes constant waveguide width (i.e. constant waveguide loss α_w) and uniform photon density along the laser cavity [5]. Nevertheless, some general conclusions on the Talbot-cavity QCLs performance can still be extracted from the comparison. In fact, both the threshold density and slope efficiency of Talbot-cavity QCL show quite close values to those of F-P device. Therefore, it is reasonable to assume that the Talbot cavity induces moderate optical loss to the QCL array, showing great potential to achieve even higher power with more devices combined. The reduced slope efficiency of the Talbot-cavity QCL compared to that of a F-P laser can be ascribed to scattering loss of Talbot cavity and self-heating effect.

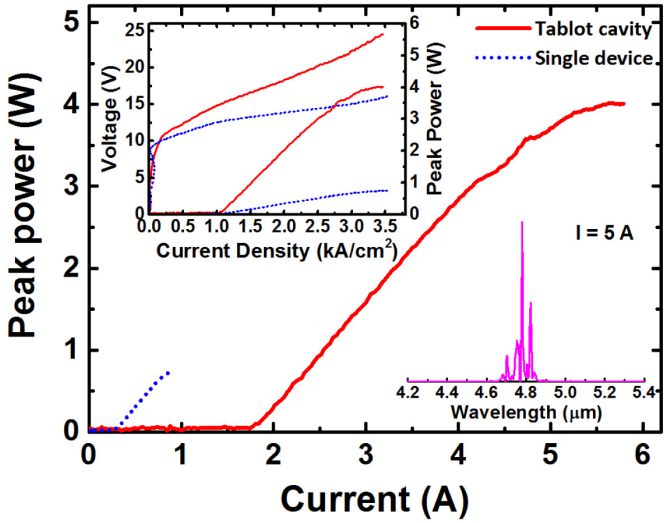

Fig. 2. Light-current (*L-I*) curves for the Talbot cavity QCL (with a Talbot cavity of Z_t /2) and a reference F-P QCL at 300 K. The upper inset shows the *L-I* and voltage current (*V-I*) curves for the same devices plotted on a current density scale. The lower inset shows the laser spectrum of Talbot-cavity QCL at a pumping current of 5 A.

The far-field distributions of the Talbot-cavity QCLs with different lengths were measured using the lock-in technique and a liquid nitrogen-cooled mercury-cadmium-telluride (MCT) detector for a better signal-to-noise ratio (SMSR). The MCT detector mounted on a rotation stage was placed ~15 cm away from the QCL array output facet and controlled by a home-built software for data collection. Figure 4 shows typical far-field distributions of Talbot-cavity QCLs with Talbot-cavity length D » 92 μm and 46 μm, corresponding to $Z_T/2$ and $Z_T/4$, respectively, at different pumping levels. The far-field distributions in Fig. 3(a) show a strong central lobe at 0°, indicating the existence of in-phase supermode operation according to couple-mode theory [8]. However, out-of-phase supermode operation appears as well. The far-field distributions in Fig. 3(b) has no lobe at center 0° position, but is primarily double lobed, showing operation of higher order supermodes.

Optics EXPRESS

However, the lobes of different supermodes overlap, making it difficult to distinguish them separately. For the in-phase supermode, theoretical analysis using the method in [17] shows a lobe spacing of ~24° between the first side lobe and the central lobe, which agrees well with the experiment value. Around roll-over point, the central lobewidth is ~5.8°, corresponding to 1.16 × diffraction limit for a 65 μm-wide aperture. We expect the far-field profile from the back facet of the laser should be similar those shown in Fig. 3, as demonstrated in the previous studies.

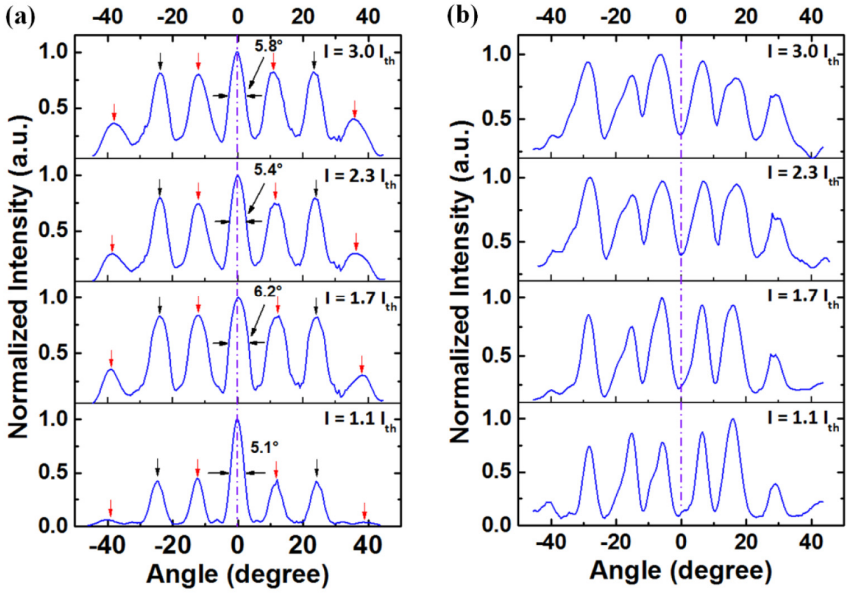

Fig. 3. (a) Far-field distribution of the Talbot-cavity QCL with $D = Z_t/2$ at different pumping levels. Side-lobes originated from the in-phase supermode are indicated by the black arrows, whereas those from the out-of-phase mode are shown by red arrows. (b) Far-field distribution of the Talbot-cavity QCL with $D = Z_t/4$ at different pumping levels.

To have a deeper understanding of the experimental results, we used the theoretical model in [18] to determine the supermode behavior of our structures. Detailed model analysis can be found in [18]. Here, we just give a brief description. In this model, the effect of the Talbot cavity is included in the effective reflectivity $N \times N$ matrix R_T at the cavity-side edge of the array region, where N is the number of lasers in the array. It is shown that $r_0^{-1}\exp(-i2\sigma D)$ is the eigenvalue λ of the matrix R_T, where r_0 is the amplitude reflectivity at the air-Talbot cavity interface, D is the channel length, and σ is the propagation constant of the supermode, given by $\sigma = (n/c)\omega - i(g_{th}/2)$. Here, c is the speed of light in vacuum, ω is the angular frequency, and g_{th} is the required threshold gain coefficient (cm^{-1}). Therefore, the threshold gain is given by $g_{th}D = \ln(1/r_0 r) + \ln(1/|\lambda|)$ [19], where r is the amplitude reflectivity at the air-array interface. Using the expression for R_T and the corresponding parameters of our current structure, the calculated threshold gains for different supermodes as a function of the Talbot cavity length is shown in Fig. 4. As shown in Fig. 4, at D » 46 μm, the in-phase supermode has the highest threshold gain, and thus the operation is severely suppressed. In this case, the laser tends to work in multiple higher order supermodes due to weak mode discrimination. For comparison, at D » 92 μm, the in-phase and out-of-phase modes have the lowest threshold gains. Hence, both supermodes are expected to lase. It is found that the $N = 4$ supermode seems to show a close gain value to that of the in-phase mode. Nevertheless, this mode is weakly observed (at ~ ± 7°) as seen in Fig. 3(a) when the laser is pumped at 1.1 I_{th}. At higher pumping currents, this mode is greatly suppressed due to laser mode competition. This can be explained that, in fact, the waveguide absorption loss of the supermodes is not considered in

Optics EXPRESS

the simplified mode which only includes the scattering loss in the Talbot cavity. Therefore, it is reasonable to assume a stronger mode discrimination at D » 92 μm for real devices, thus suppressing the operation of $N = 4$ supermode which should be observed at high currents with side peaks at ~ ± 7°. Though straightforward, the studied model qualitatively matches the experiment findings.

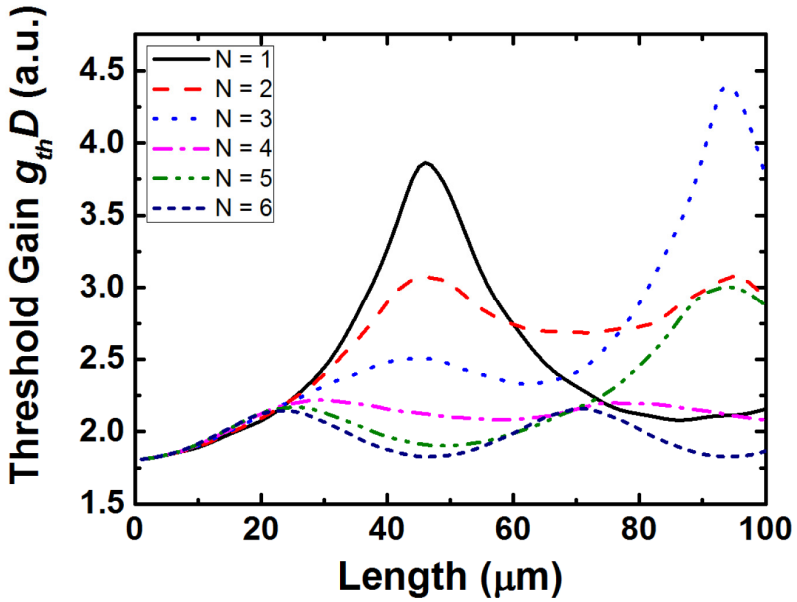

Fig. 4. Theoretical threshold gain for the supermodes of a six-element Talbot-cavity QCL array as a function of the Talbot cavity length. The $N = 1$, corresponds to the in-phase supermode, whereas the $N = 6$ is the out-of-phase supermode.

4. Conclusion

In conclusion, we have demonstrated mid-infrared six-element Talbot-cavity quantum cascade lasers with coherent emission. Maximum output power of ~4 W was achieved, which scales almost linearly with the number of the device in the array. In-phase supermode operation has been demonstrated with a near diffraction limit of the far-field distribution in the central lobe over the whole dynamic range. The proposed approach holds the potential to circumvent the main limitations on the high power CW QCLs. Further studies should be taken to increase the mode discrimination so as to achieve pure in-phase supermode operation and thus high brightness which is important for practical applications. Possible approaches to further improve the device performance include Tablot-cavity array with separate contacts [20], novel array configuration [21], or tilted Talbot-cavity output facet [22]. Meanwhile, further reducing the array period will be beneficial for reducing the side peak intensity, thus leading to a higher side mode suppression ratio (SMSR) for in-phase supermode.

Funding

National Research Foundation Singapore (NRF), Competitive Research Program (NRF2015 NRF-CRP002-008); Ministry of Education – Singapore (MOE) Tier 2 program (MOE2016-T2-1-128).

Acknowledgment

At the time of writing this manuscript, we noted an independent work [23] was carried out in parallel using three laser elements, with a wider ridge width and period.